

# High-fidelity quantum operations on superconducting qubits in the presence of noise

Andrew J. Kerman and William D. Oliver

Lincoln Laboratory, Massachusetts Institute of Technology, Lexington, MA, 02420

(Dated: April 14, 2019)

We present a scheme for implementing quantum operations with superconducting qubits. Our approach uses a “coupler” qubit to mediate a controllable, secular interaction between “data” qubits, pulse sequences which strongly mitigate the effects of  $1/f$  flux noise, and a high-Q resonator-based local memory. We develop a Monte-Carlo simulation technique capable of describing arbitrary noise-induced dephasing and decay, and demonstrate in this system a set of universal gate operations with  $\mathcal{O}(10^{-5})$  error probabilities in the presence of experimentally measured levels of  $1/f$  noise. We then add relaxation and quantify the decay times required to maintain this error level.

PACS numbers: 02.70.Ss, 03.65.Yz, 03.67.Ac, 03.67.Lx, 03.67.Pp, 85.25.Am, 85.25.Cp

Superconducting qubits are promising building blocks for quantum computers [1]. Realizing this promise requires a qubit coupling scheme and associated control pulse sequences capable of realizing gate operations with error probabilities low enough to achieve fault-tolerance [2]. Such a control scheme should ideally permit a practical (as opposed to optimal), time-efficient implementation of universal single- and two-qubit operations; incorporate switchable coupling between qubits; and be insensitive both to decoherence and fabrication variations of the qubits.

Although several proposed [3, 4, 5, 6] and experimental [7] qubit coupling schemes already exist, none yet combine all of the above features. In this Letter, we present a scheme which aims to do this. Our approach utilizes a “coupler” qubit to mediate interaction between “data” qubits [4], pulse sequences incorporating spin-echoes to suppress the effects of  $1/f$  flux noise [8, 9], and local memory in the form of high-Q resonators [10]. We introduce a quantum Monte-Carlo technique capable of simulating gate operations in the presence of noise and spontaneous decay, which we then use to show that  $\mathcal{O}(10^{-5})$  error probabilities (comparable to certain predicted thresholds for fault-tolerance [2]) can be achieved in the presence of experimentally measured levels of flux noise. Finally, we quantify the qubit excited-state lifetimes and control signal requirements necessary to achieve this.

We focus here on the flux qubit [11], although much of what follows is more generally applicable. In most work to date, this consists of a single superconducting loop interrupted by several Josephson junctions [Fig. 1(b)]. In this work, however, we consider the double-loop four-junction version [Fig. 1(c)]. When  $\Phi_1, \Phi_2 \approx \frac{\Phi_0}{2}, 0$  ( $\Phi_0 = h/2e$  is the flux quantum), the qubit can be described by the approximate two-level Hamiltonian  $\hat{H}_{\text{qb}} = \frac{1}{2}[\epsilon\hat{\sigma}^z + \Delta\hat{\sigma}^x]$ . The eigenstates of  $\hat{\sigma}^z$  are “persistent current” (PC) states with energies  $\pm\epsilon/2 = \pm I_p(\Phi_1 - \frac{\Phi_0}{2})$ , where currents  $\pm I_p$  circulate around the  $\Phi_1$  loop. The parameters  $\epsilon$  and  $\Delta$  are tunable by the fluxes  $\Phi_\epsilon \equiv \Phi_1 + \frac{\Phi_2}{2}$  and  $\Phi_\Delta \equiv \Phi_2$  [Figs. 1(c),(f)]. Point A in Fig. 1(a), where the PC states are mixed to produce an avoided

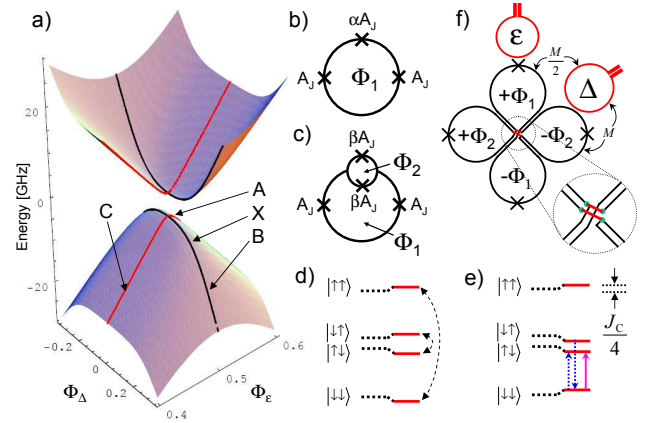


FIG. 1: (color online) Flux qubits and secular vs. nonsecular coupling. (a) Lowest-two energy levels for a flux qubit. Schematic of (b) single-loop 3-JJ and (c) double-loop 4-JJ flux qubits. Relative junction areas have ratios  $\alpha$  and  $\beta$  [11]. Single-loop qubits have only one control flux  $\Phi_\epsilon$  and are restricted to the line AC in (a). Double-loop qubits have two control fluxes:  $\Phi_\epsilon \equiv \Phi_1 + \frac{\Phi_2}{2}$  and  $\Phi_\Delta \equiv \Phi_2$ . (d) Energy levels for two flux qubits at degeneracy, with nonsecular coupling. Level shifts result from second-order mixing of two-qubit eigenstates (dashed arrows). (e) Energy levels for secular coupling. A conditional level shift allows CNOT to be implemented with a single microwave transition (solid arrow), and SWAP with a stimulated Raman transition (by driving a  $2\pi$  pulse on each qubit, corresponding to a  $\pi$  pulse on the Raman transition). (f) “Cloverleaf” 4-JJ qubit, gradiometric in both loops.  $\Phi_1$  and  $\Phi_2$  can be accessed independently. The  $\Delta$  control-loop orientation induces  $\Phi_1$  and  $\Phi_2$  in the -0.5:1 ratio required to adjust  $\Delta$  without affecting  $\epsilon$ .

crossing with  $\hat{\sigma}^x$ -like energy eigenstates, is known as the “degeneracy point”. It has the desirable feature that  $dE/d\Phi_\epsilon = dE/d\Phi_\Delta = 0$  (where the qubit energy splitting  $E = \sqrt{\epsilon^2 + \Delta^2}$ ) so that decoherence due to flux noise is minimized [8]. Existing qubit coupling schemes which are insensitive to decoherence rely on biasing at this point [3, 4, 5].

There are, however, two disadvantages to working at degeneracy: first,  $E$  is then fixed by fabrication and may vary significantly between qubits, requiring individually

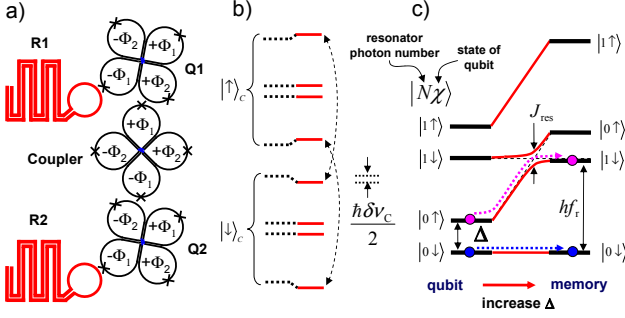


FIG. 2: (color online) Scheme for universal two-qubit operations. (a) A 4-JJ coupler qubit mediates the interaction between two 4-JJ data qubits (Q1, Q2). Coupling is switched off by tuning  $\epsilon_C \gg \Delta_C$ . (b) An inductive interaction mixes the coupler levels (dashed arrows), resulting in a conditional frequency shift  $\delta\nu_C$  in the computational subspace  $C_2$  [see Fig. 1(e)] [13]. (c) Increasing the qubit  $\Delta$  adiabatically through the qubit-resonator avoided crossing transfers the qubit state to the resonator [10].

tuned microwaves; second, the degenerate qubit is first-order insensitive to flux from other qubits, so that inductively coupling  $\Phi_1$ -loops, as in previous works [3, 4, 5], has no effect on the system to first order. This “nonsecular” coupling can be written in the form  $\hat{H}_C^{zz} \equiv J_C^{zz} \hat{\sigma}_1^z \hat{\sigma}_2^z$  (the subscripts indicate qubits 1 and 2), and its leading-order effect at degeneracy is a second-order mixing [Fig. 1(d)]. This mixing can be exploited using double resonance [3] or parametric driving [4, 5] to enable, for example, the two-qubit  $\sqrt{\text{SWAP}}$  gate, even if the qubits have different splittings [3, 4, 5]; however, these schemes require different microwave frequencies either for each qubit or qubit pair. Furthermore, the Controlled-NOT (CNOT) gate used ubiquitously in quantum circuits must then be constructed from several  $\sqrt{\text{SWAP}}$  and single-qubit gates [12].

Far from degeneracy ( $\epsilon \gg \Delta$ ), however, the energy eigenstates are approximately PC states, and  $\hat{H}_C^{zz}$  commutes with  $\hat{H}_{qb}$ , giving a first-order level shift [Fig. 1(e)] which lifts the degeneracy between the  $|\downarrow\downarrow\rangle \leftrightarrow |\uparrow\downarrow\rangle$  and  $|\downarrow\uparrow\rangle \leftrightarrow |\uparrow\uparrow\rangle$  transitions by the conditional frequency shift  $\hbar\delta\nu_C = J_C^{zz}$ . This “secular” coupling allows a CNOT to be driven with a single microwave pulse (Fig. 1(e), solid arrow), and SWAP with a stimulated Raman transition (dashed arrows). However, the qubits are now sensitive to flux noise due to the large, nonzero slope  $dE/d\Phi_\epsilon = 2I_p$ .

Based on these observations, we consider the system shown in Fig. 2(a) consisting of two two-loop “data” qubits, whose coupling is mediated by a third “coupler” qubit in a manner similar to that used in Ref. 4 for single-loop qubits. Here, however, we inductively couple to  $\Phi_\Delta$  of each data qubit rather than  $\Phi_1$  (as in previous works), with the Hamiltonian:  $\hat{H}_C = J_C \hat{\sigma}_C^z (\hat{\sigma}_1^x + \hat{\sigma}_2^x)$ , where  $J_C \approx M_{iC} I_p d\Delta_i / d\Phi_S$  and  $M_{iC}$  is the mutual inductance between data and coupler qubits. When  $\epsilon_1 = \epsilon_2 = \epsilon_C = 0$ ,

this configuration produces the level structure shown in Fig. 2(b). The lower four of these eight eigenstates (hereafter the two-qubit “computational subspace” or  $C_2$ ) exhibit an effective two-qubit conditional frequency shift  $\hbar\delta\nu_C = \Delta_C \{1 - \sqrt{1 + (2J_C/\Delta_C)^2}\}$  equivalent to that shown in Fig. 1(e) [13]. In addition, this shift can be turned off by tuning  $\epsilon_C/\Delta_C \gg 1$ , so that the coupler eigenstates become approximately PC states (and eigenstates of  $\hat{H}_C$ ); this suppresses the mixing shown in Fig. 2(b), and with it  $\delta\nu_C$  by the factor  $\sim (\Delta_C/\epsilon_C)^3$ . The speed of this switching is limited only by nonadiabatic excitation of the coupler qubit [14]. Finally, the sensitivity of each data qubit to flux noise in this configuration is given by  $d\Delta/d\Phi_\Delta = J_C/M_{iC} I_p^C$  ( $I_p^C$  is the coupler persistent current), which can be reduced substantially by using larger junctions in the coupler qubit to increase  $I_p^C$ .

The final ingredient shown in Fig. 2(a) are the transmission-line resonators coupled to the  $\Phi_\epsilon$ -loop of each qubit so that its state can be adiabatically transferred into a resonator state [10] [Fig. 2(c)]. These resonators provide a potentially long-lived memory in which qubit states can be stored between manipulations.

To simulate our system, we integrate the time-dependent Schrödinger equation with the Hamiltonian:

$$\hat{H} = \frac{1}{2} \sum \{[\epsilon_i(t) + \hbar\Omega_{\mu i}(t) \cos(\omega_i t)] \hat{\sigma}_i^z + \Delta_i(t) \hat{\sigma}_i^x\} + \sum [hf_{rj} \hat{a}_{rj}^\dagger \hat{a}_{rj} + J_{\text{res}} (\hat{a}_{rj}^\dagger + \hat{a}_{rj}) \hat{\sigma}_j^z] + \hat{H}_C \quad (1)$$

where  $i \in \{1, 2, C\}$ ,  $j \in \{1, 2\}$ , and we have added microwave fields illuminating the  $\Phi_\epsilon$  loop of each qubit. We treat the qubits as two-level systems and truncate the ladder of resonator photon states at  $n = 1$  [14]. As fixed input parameters, we assume resonator frequencies  $f_{r1, r2} = 9, 11$  GHz (they may be identical in general), qubit-resonator coupling  $J_{\text{res}}/\hbar = 0.75$  GHz, and qubit-qubit coupling  $J_C/\hbar = 0.3$  GHz [15].

We have simulated Hadamard (H), CNOT, and SWAP gates. As an example, the CNOT pulse sequence is shown in Fig. 3(a). Both qubits begin with states stored in their respective resonators ( $\Delta_{1,2}$  high), and with the coupler “off” ( $\epsilon_C/\Delta_C \gg 1$ ). A downward ramp is applied to both  $\Delta_i$  to retrieve the qubits’ states (only one  $\Delta_i$  would be ramped for H). These ramps are optimized to maintain a constant non-adiabaticity as the avoided crossing in Fig. 2(c) is traversed. Next, the qubits are manipulated with single-qubit microwave rotations and conditional phase (C $\Phi$ ) gates produced by transiently pulsing the coupler “on” ( $\epsilon_C/\Delta_C = 0$ ) using linear flux ramps [14]. The CNOT pulse sequence (with bit 1 the target qubit) shown in Fig. 3(a) is:  $R_{1,2}(\pi) R_1^x(\frac{\pi}{2}) C^e(\frac{\pi}{2}) R_1^y(\frac{\pi}{2}) C^e(\frac{\pi}{2}) R_{1,2}(\pi)$ , where  $R_{p,q}^\nu(\theta)$  is a rotation of angle  $\theta$  around axis  $\nu$  on the Bloch sphere for qubits  $p$  and  $q$ ,  $C^e(\frac{\pi}{2}) \equiv C(\frac{\pi}{4}) R_{1,2}(\pi) C(\frac{\pi}{4})$ , and we have suppressed the free evolution intervals for clarity. The  $\pi$ -pulses induce spin-echoes at the center of each  $\pi/2$ -pulse and at the end of

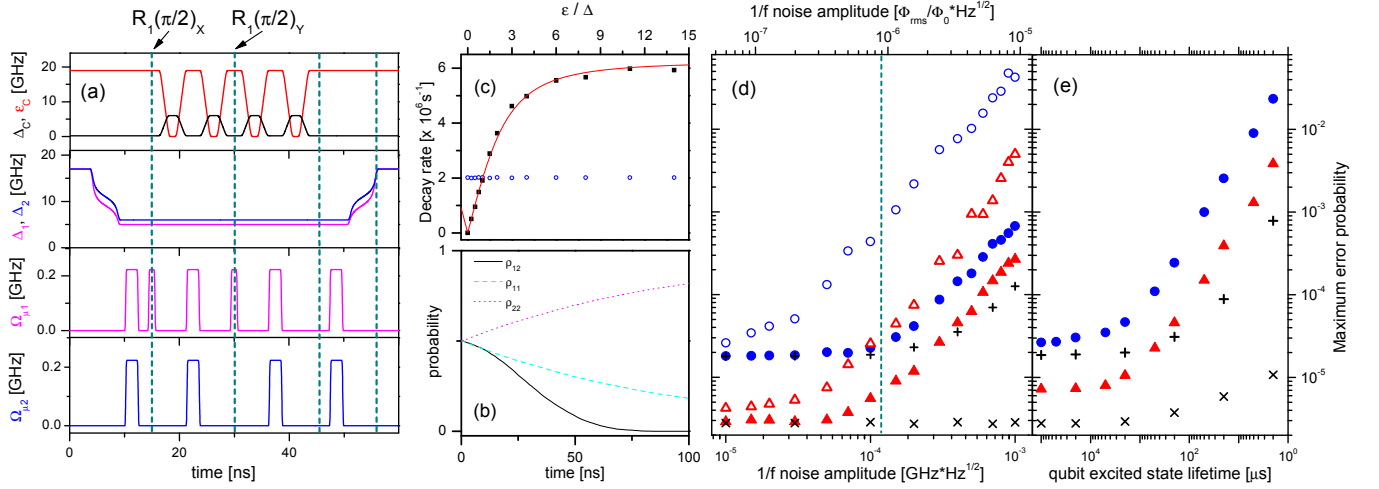


FIG. 3: (color online) Simulation of gate operations in the presence of noise. (a) CNOT pulse sequence. Data qubits are ramped to  $\Delta_{1,2} = 5, 6$  GHz during operations, e.g., point X [Fig. 1(a)] ( $\Delta_{1,2}$  are chosen to be different here only for clarity); the coupler has  $(\epsilon_C, \Delta_C) = (17, 0.2)$  GHz and  $(0, 4)$  GHz in the decoupled and coupled states, respectively [15]. Pulsed microwaves generate  $\pi$  and  $\pi/2$  rotations;  $C\pi/4$  operations are generated by coupling for a controlled duration. Spin-echoes are generated at times indicated by dashed lines using  $\pi$ -pulses. (b) Simulation of a single qubit including  $1/f$  noise and spontaneous decay (see text). (c) Decay rates as a function of  $\epsilon/\Delta$ . Solid symbols show the fitted exponential decay rate  $\Gamma_e$  of  $\rho_{22}$  (constant by construction). Open symbols show the decay rate  $\Gamma_g$ , extracted by fitting  $|\rho_{12}|$  to the approximate expression:  $\exp[-\Gamma_e t - (\Gamma_g t)^2]$  with  $\Gamma_e$  fixed at the fitted value. The solid red line is based on the theory in Ref. [19] with no free parameters. (d) maximum gate error  $\mathcal{E}$  for H (triangles) and CNOT (circles) gates with  $T_1 \rightarrow \infty$  and noise spectral density  $S(\omega) = A_\omega/\omega$ , vs.  $A_\omega$ . Open symbols: same operations without spin-echo compensation. Vertical dashed line: experimentally measured noise level of  $1 \mu\Phi_0/\sqrt{\text{Hz}}$  at 1 Hz [8]. (e) Maximum error probabilities at that noise level versus the qubits' excited state lifetime. In both (d) and (e), (+) and (x) show  $\mathcal{E}$  for CNOT and H, respectively, with noise and decay on the coupler qubit only.

the operation. H and SWAP can be constructed similarly:  $H = R_1(\pi)R_{1,2}^x(\frac{\pi}{2})R_1(\pi)$ , and  $\text{SWAP} = R_{1,2}(\pi)R_{1,2}^x(\frac{\pi}{2})C^e(\frac{\pi}{2})R_{1,2}^y(\frac{\pi}{2})C^e(\frac{\pi}{2})R_{1,2}^x(\frac{\pi}{2})C^e(\frac{\pi}{2})R_{1,2}(\pi)$ . Finally, the qubit states are transferred back into the resonators, and the final relative phase of each qubit is adjusted by varying the time at which this occurs.

All microwave pulses have a fixed amplitude (with 100-ps rise/fall times), so that pulse area is controlled solely by their duration. This is crucial for producing effective spin-echoes with short, intense pulses at a fixed frequency, due to the Bloch-Siegert shift. This frequency shift is amplitude dependent, so the microwave amplitude must be kept fixed in order to compensate for it with a fixed frequency offset (here,  $\sim 5$  MHz).

The use of single-qubit rotations and  $C\Phi$  gates instead of the frequency-resolved pulses shown in Fig. 1(e) has several advantages: first, it requires only a single microwave frequency for all operations (assuming all qubits are tuned to the same frequency using  $\Phi_\Delta$ ); second, it does not require accurately resolving two frequencies spaced by  $\delta\nu_C$  using long microwave pulses [16]. Finally, all gate parameters can be adjusted solely by varying the timing of the microwave and flux pulse edges.

We simulate the effect of decoherence due to flux noise using a Monte-Carlo technique. Noise is added to each  $\Delta_i$  and  $\epsilon_i$  in eq. 1 by superposing an independent, discrete set of random two-level “telegraph” signals [17], which produce a  $1/f$  average spectral density. For each

Monte-carlo iteration (all of which can be run in parallel), a new set of noise functions is generated (one for each  $\epsilon, \Delta$ ). From these we obtain a sequence of  $N$  time intervals  $\{\delta\tau_i\}$  (typically  $N \sim$  several hundred) whose union is the full gate time, and over each of which all fluctuators are *constant*. We then integrate the 32 coupled Schrödinger equations sequentially over these intervals. The final states for all iterations are converted to density matrices and then averaged, corresponding to a statistical mixture of the different noise realizations.

Spontaneous decay is added as follows. At the end of each  $\delta\tau_i \equiv t_i - t_{i-1}$ , we construct the density matrix  $\rho_i$  and apply amplitude damping to the qubits:  $\rho_i^\gamma = \mathcal{S}^1(\gamma_i)\mathcal{S}^2(\gamma_i)\mathcal{S}^C(\gamma_i)\rho_i$  where  $\mathcal{S}^j(\gamma)\rho = \sum_k U_k^j(\gamma)\rho U_k^j(\gamma)^\dagger$ , and:

$$U_{1,2}^j(\gamma) = M_d^j \left\{ \begin{pmatrix} 1 & 0 \\ 0 & \sqrt{1-\gamma} \end{pmatrix}, \begin{pmatrix} 0 & 0 \\ \sqrt{\gamma} & 0 \end{pmatrix} \right\} (M_d^j)^\dagger. \quad (2)$$

Here,  $\gamma_i = 1 - \exp[-\delta\tau_i/T_1^j]$  is the probability of decay for qubit  $j$  during  $\delta\tau_i$ ,  $T_1^j$  is the excited-state decay time for qubit  $j$ , and  $M_d^j$  transforms from the instantaneous energy eigenbasis of the *isolated* qubit  $j$  at time  $t_i$  (decay is assumed to occur in this basis) to the fixed basis of the simulation [18]. To return to state-vector space at the end of each  $\delta\tau_i$ , we first write  $\rho_i = \sum_k \lambda_i^k |\psi_i^k\rangle\langle\psi_i^k|$ . In principle, we could then pick one normalized  $|\psi_i^k\rangle$  at random according to the probabilities  $\lambda_i^k$ ; however, since  $\lambda_i^k \leq$

$\mathcal{O}(\gamma_i)$  for  $k \neq 1$  (with  $\lambda_i^k$  in decreasing order for given  $i$ ), convergence of the Monte-Carlo sum would require many iterations to sample enough of these unlikely events. Instead, we use an expansion procedure to speed up this convergence. For each noise realization, we simulate two leading terms (i) and (ii) in a weighted Monte-Carlo sum: for (i), we choose  $|\psi_i^1\rangle$  for all times  $t_i \in \{t_1 \cdots t_N\}$ ; the probability for this to occur is  $\mathcal{P}_0 \equiv \prod_i \lambda_i^1$ . For (ii), we choose instead a sequence of eigenvectors of the form:  $\{\psi_1^1, \dots, \psi_{n-1}^1, \psi_n^m, \psi_{n+1}^1, \dots, \psi_N^1\}$  with  $m \neq 1$ , an event whose probability is  $\mathcal{P}(m, n) \equiv \mathcal{P}_0 \lambda_n^m / \lambda_n^1$ . We choose  $\{m, n\}$  randomly according to the probabilities  $\mathcal{P}(m, n) / \mathcal{P}_1$ , where  $\mathcal{P}_1 \equiv \sum_{m, n} \mathcal{P}(m, n)$ . The final density matrices from (i) and (ii) are then averaged with the relative weightings  $\mathcal{P}_0$  and  $\mathcal{P}_1$ .

Figures 3(b) and (c) show a test of this method on a single qubit initially in the state  $(|\uparrow\rangle + |\downarrow\rangle) / \sqrt{2}$ , under the influence of both 1/f noise and decay. As expected, the excited state decays exponentially, while the coherence does not [Fig. 3(b)]. Decay rates can be extracted from these data, and are shown in Fig. 3(c) as a function of  $\epsilon / \Delta$ . The solid line is a prediction, with no free parameters, using the theory from Ref. 19.

To fully characterize a gate operation, we run the simulation (in parallel) for each of a set of chosen initial states  $|\phi_0^\nu\rangle$  spanning  $\mathcal{C}_2$ . These outputs can be used to reconstruct the superoperator  $\mathcal{S}_{\text{op}}$  for the gate (acting on density matrices in  $\mathcal{C}_2$ ), which can be represented as a 16 x 16 matrix acting on “vectors” obtained by stacking the columns of the 4 x 4 density matrix [20]. For decoherence only (no decay), each iteration can be written as a unitary operation in  $\mathcal{C}_2$ , and only four  $|\phi_0^\nu\rangle$  are required to reconstruct  $\mathcal{S}_{\text{op}}$ . With decay, however, this is no longer true due to the projection and renormalization, and *sixteen*  $|\phi_0^\nu\rangle$  are required.

For a given operation, we calculate the maximum error probability:  $\mathcal{E} = 1 - \min [\langle \Psi | \mathcal{S}_0^{-1} \mathcal{S}_{\text{op}} \rho | \Psi \rangle]$ , where  $\mathcal{S}_0$  is the superoperator corresponding to the desired operation, and maximization is over normalized state vectors  $|\Psi\rangle$  in  $\mathcal{C}_2$ . Figure 3(d) shows  $\mathcal{E}$  for the CNOT (circles) and Hadamard (triangles) gates, both with spin-echo compensation [fig. 3(a)] (filled symbols) and without it (open symbols), as a function of 1/f-noise amplitude  $A_\omega$ , for  $T_1 \rightarrow \infty$  [21, 22]. The spin-echo compensation strongly suppresses errors due to 1/f noise, keeping  $\mathcal{E}$  at or below  $\mathcal{O}(10^{-5})$  up to the noise level observed in Ref. 8, indicated by the vertical dashed line. Figure 3(e) shows  $\mathcal{E}$  for this same noise level as a function of the qubits’ excited state lifetime, which would evidently have to be  $\sim$  ms for  $\mathcal{E} \sim 10^{-5}$ . Finally, (+) and (x) show  $\mathcal{E}$  with noise and decay added only to the coupler qubit, illustrating that although the extra qubit does in principle expose the system to more noise, the present configuration is insensitive to it.

Although  $\mathcal{E}$  can be used to set bounds on fault-tolerance thresholds for quantum circuits, the  $\mathcal{S}_{\text{op}}$  generated by these simulations give much more: a full statistical description of the errors that occur for an arbitrary input state. This may provide a means to compute more accurate thresholds for real quantum circuits (assuming that noise correlations between successive operations can be neglected). Furthermore, it may enable the design of optimized error-correction schemes and/or gate operation protocols which target a particular noise source, enabling higher thresholds for fault-tolerance.

This work is sponsored by the United States Air Force under Air Force Contract #FA8721-05-C-0002. Opinions, interpretations, recommendations and conclusions are those of the authors and are not necessarily endorsed by the United States Government.

- 
- [1] Y. Makhlin, G. Schön, A. Shnirman, Rev. Mod. Phys. **73**, 357 (2001).
  - [2] See, e.g.: A.M. Steane, Phys. Rev. A **68**, 42322 (2003); P. Aliferis, D. Gottesman, and J. Preskill, Quant. Inf. Comput. **6**, 97 (2006); K.M. Svore, D.P. DiVincenzo, and B.M. Terhal, Quant. Inf. Comput. **7**, 297 (2007).
  - [3] C. Rigetti, A. Blais, and M. Devoret, Phys. Rev. Lett. **94**, 240502 (2005); S. Ashhab, S. Matsuo, N. Hatnaka, and F. Nori Phys. Rev. B **74**, 184504 (2006).
  - [4] A.O. Niskanen, Y. Nakamura, and J.-S. Tsai, Phys. Rev. B **73**, 094506 (2006).
  - [5] P. Bertet, C.J.P.M. Harmans, and J.E. Mooij, Phys. Rev. B **73**, 064512 (2006).
  - [6] B.L.T. Plourde, *et al.*, Phys. Rev. B **70**, 140501(R) (2004); A. Maassen van den Brink, A.J. Berkley, and M. Yalowsky, New J. Phys. **7**, 230 (2005); A. Blais, *et al.*, Phys. Rev. A **75**, 032329 (2007); Y. Liu, L.F. Wei, J.S. Tsai, and F. Nori, Phys. Rev. Lett. **96**, 067003 (2006).
  - [7] T. Hime, *et al.*, Science **314** 1427 (2006); S.H.W. van der Ploeg, *et al.*, Phys. Rev. Lett. **98**, 057004 (2007).
  - [8] F. Yoshihara, K. Harrabi, A.O. Niskanen, Y. Nakamura, and J.S. Tsai, Phys. Rev. Lett. **97**, 167001 (2006).
  - [9] K. Kakuyanagi, *et al.*, Phys. Rev. Lett. **98**, 047004 (2007).
  - [10] R.H. Koch, *et al.*, Phys. Rev. Lett. **96** 127001 (2006).
  - [11] T.P. Orlando, *et al.*, Phys. Rev. B **60**, 15398 (1999).
  - [12] N. Shuch and J. Siewert, Phys. Rev. A **67**, 032301 (2003); M.J. Bremner, *et al.*, Phys. Rev. Lett. **89**, 247902 (2002).
  - [13] The level structure in Fig. 2(b) also has the property that the parity of the two-qubit state can be directly measured using the coupler energy splitting, which could be useful for error-correction.
  - [14] We simulated the full single-qubit dynamics ( $\pm 16$  charge states) under the action of flux and microwave pulses; slew rates, relative timing, and microwave amplitudes for all pulses were chosen to keep nonadiabatic and off-resonant microwave excitation out of the lowest two states below  $10^{-5}$ . We checked the  $n_{ph} = 1$  truncation of resonator photon states by simulating up to  $n_{ph} = 3$ .
  - [15] We assumed the following physical values: Data qubits:  $E_J/h = 175$  GHz,  $I_p = 250$  nA,  $E_J/E_C = 40$ ,  $\beta = 0.925$ , and  $\Phi_\Delta = 371$  m $\Phi_0$ ; Coupler qubit:  $E_J/h = 350$  GHz,

- $I_p = 500$  nA,  $E_J/E_C = 160$ ,  $\beta = 0.375$ ;  $(\Phi_\epsilon, \Phi_\Delta) = (0, 179)$  m $\Phi_0$  and  $(5.44, 0)$  m $\Phi_0$  for the coupled and uncoupled states. Then,  $M_{iC} = 10$  pH gives  $J_C \approx 2\pi \times 0.3$  GHz.
- [16] These short, spectrally broad microwave pulses are also less sensitive to microwave frequency (phase) noise.
  - [17] For each  $\epsilon$  and  $\Delta$ , we used 40 independent fluctuators, with average switching rates spaced logarithmically from  $\nu_{ir} = 1$  Hz to  $\nu_{uv} = 0.2$  GHz, and relative amplitudes chosen to maximize convergence to a  $1/f$  spectrum. Net amplitudes are determined by the slopes  $d\epsilon/d\Phi_\epsilon$  and  $d\Delta_i/d\Phi_\Delta$ . Error rates do depend on  $\nu_{ir}$  as expected [19], but are independent of  $\nu_{uv}$  for  $\nu_{uv} \geq 0.2$  GHz.
  - [18] We explicitly neglect any cooperative effects in decay, although these could be readily included.
  - [19] G. Ithier, *et al.*, Phys. Rev. B **72**, 134519 (2005).
  - [20] I.L. Chuang and M.A. Nielsen, J. Mod. Opt. **44**, 2455 (1997); J.F. Poyatos, J.I. Cirac, and P. Zoller, Phys. Rev. Lett. **78**, 390 (1997); T.F.Havel, J. Math. Phys. **44**, 534 (2003).
  - [21] Our simulations also allow us to determine the control-pulse requirements for  $\mathcal{E} \sim 10^{-5}$ . For  $\Omega_\mu(t)$ ,  $\epsilon_C(t)$ , and  $\Delta_C(t)$ : 8 bit vertical accuracy, 1 ps edge timing; for  $\Delta_1(t)$  and  $\Delta_2(t)$ , 14 bit, 0.2 ps. The latter pair can be relaxed by reducing the qubit-resonator detuning; however, this would also increase off-resonant mixing between them and reduce the resonator lifetime. Removing the resonators entirely is also possible, and will be considered in a future publication.
  - [22] The error “floor” for  $A_\omega \rightarrow 0$  is caused by residual nonadiabaticity in the qubit-resonator quantum-state transfer.